Biophysical Journal Volume 108 June 2015 2816–2824

Article

Orientation and Order of the Amide Group of Sphingomyelin in Bilayers Determined by Solid-State NMR

Nobuaki Matsumori,[1,*] Toshiyuki Yamaguchi,[1,2] Yoshiko Maeta,[1] and Michio Murata[1,2]

[1]Department of Chemistry and [2]Japan Science and Technology Agency, ERATO, Lipid Active Structure Project, Graduate School of Science, Osaka University, Osaka, Japan

ABSTRACT Sphingomyelin (SM) and cholesterol (Chol) are considered essential for the formation of lipid rafts; however, the types of molecular interactions involved in this process, such as intermolecular hydrogen bonding, are not well understood. Since, unlike other phospholipids, SM is characterized by the presence of an amide group, it is essential to determine the orientation of the amide and its order in the lipid bilayers to understand the nature of the hydrogen bonds in lipid rafts. For this study, 1′-^{13}C-2-^{15}N-labeled and 2′-^{13}C-2-^{15}N-labeled SMs were prepared, and the rotational-axis direction and order parameters of the SM amide in bilayers were determined based on ^{13}C and ^{15}N chemical-shift anisotropies and intramolecular ^{13}C-^{15}N dipole coupling constants. Results revealed that the amide orientation was minimally affected by Chol, whereas the order was enhanced significantly in its presence. Thus, Chol likely promotes the formation of an intermolecular hydrogen-bond network involving the SM amide without significantly changing its orientation, providing a higher order to the SM amide. To our knowledge, this study offers new insight into the significance of the SM amide orientation with regard to molecular recognition in lipid rafts, and therefore provides a deeper understanding of the mechanism of their formation.

INTRODUCTION

Since the lipid rafts hypothesis was first proposed in the late 1990s (1), the formation of microdomains in biomembranes has been investigated because of its implications for membrane processes such as signal transduction, protein sorting, and microbial infection (2–6). Lipid rafts are thought to be associated with a liquid-ordered phase, which is characterized by tight packing but relatively high lateral lipid mobility. In contrast, unsaturated phosphatidylcholines (PCs) are loosely packed and develop a liquid-disordered phase that coexists with the liquid-ordered domain under certain conditions. In general, cholesterol (Chol) and sphingolipids such as sphingomyelin (SM) are considered essential for the formation of lipid rafts (7–9).

The structure of SM is characterized by the presence of amide and hydroxy groups, which presumably are responsible for the formation of collateral intra- and intermolecular hydrogen bonds in membranes, making SM a preferable raft constituent compared with PC. Numerous theoretical and experimental studies have been conducted in an attempt to reveal the nature of the interactions involving the amide and hydroxy groups of SMs. For example, in lipid bilayers the SM amide group has been reported to interact with water, the hydroxy and amide groups of other SM molecules, and the hydroxy group of Chol, and possible hydrogen bonding with Chol has drawn the most attention as a key factor in raft formation (10–14). However, the detailed nature of the molecular interaction, including hydrogen bonds in the SM bilayers, has not been fully elucidated due to limited experimental data on SM conformation and dynamics.

Recently, Yamaguchi et al. (15) determined the partial conformation of an SM molecule in a membrane environment using bicelles as a raft model, revealing that its conformation is relatively stable and capable of forming intermolecular hydrogen bonds between amide groups. In addition, the comprehensive and unambiguous order profiles of the SM alkyl chains were recently determined using site-specifically deuterated SMs (16,17). The results demonstrated a higher thermal stability of the upper portions of the acyl chains, which further suggests intermolecular hydrogen-bond formation between SM amides. To gain further insights into the hydrogen bonding involving the SM amides, detailed information about the dynamic and spatial properties of the amide moiety in a bilayer membrane is required.

In previous studies (18,19), we reported the rotation-axis direction and order parameter of 6-F-Chol in PC and SM bilayers by analyzing ^{19}F chemical shift anisotropy (CSA) and intramolecular ^{13}C-^{19}F dipole coupling constants in conjunction with ^{2}H NMR data. This method can be applied to analyze the orientation of the SM amide plane in lipid bilayers. Hence, we prepared two types of ^{13}C/^{15}N doubly

Submitted August 29, 2014, and accepted for publication May 11, 2015.

*Correspondence: matsmori@chem.kyushu-univ.jp

Nobuaki Matsumori's present address is Department of Chemistry, Graduate School of Science, Kyushu University, Higashi-ku, Fukuoka 812-8581, Japan.

Editor: Klaus Gawrisch.

0006-3495/15/06/2816/9 $2.00

http://dx.doi.org/10.1016/j.bpj.2015.05.011

labeled SMs, 1′-^{13}C-2-^{15}N-SM and 2′-^{13}C-2-^{15}N-SM (Fig. 1), for this study and analyzed ^{13}C and ^{15}N CSAs, as well as intramolecular ^{13}C-^{15}N dipole coupling constants, to determine the rotational-axis direction and order parameter of the SM amides in bilayer membranes with and without Chol. In this study, we used 50 mol % Chol to ensure the formation of the ordered phase as well as to make the condition identical to that used in our previous study on the order profile of SM alkyl chains (16,17).

MATERIALS AND METHODS

Details regarding the synthetic procedures used for the ^{13}C/^{15}N doubly labeled SMs and calculations of CSA tensors are described in the Supporting Material.

Sample preparation and solid-state NMR measurements

For static CSA measurements of SM amides, powdered 1′-^{13}C-SM or 2-^{15}N-SM (10.8 mg, 14.8 μmol), prepared in the same manner as the ^{13}C/^{15}N doubly labeled SMs, was transferred into a 5-mm magic-angle spinning (MAS) rotor. For preparation of membrane samples, labeled SM (8.0 mg, 10.9 μmol) with or without Chol (4.2 mg, 10.9 μmol) was dissolved in MeOH-$CHCl_3$ and the solvent was removed under vacuum for at least 12 h. The dried membrane film was hydrated with 1 mL of water. After a few minutes of sonication (Branson 1510 ultrasonic cleaner (Danbury, CT)) and vortexing (Voltex-2Genie (Scientific Industries, Bohemia, NY)) at 55°C, the suspension was freeze-thawed three times to make multilamellar vesicles. Then the vesicle solution was lyophilized and rehydrated with 8 μL (for SM membranes) or 12.2 μL (for SM-Chol membranes) using deuterated water. The suspension was vortexed and freeze-thawed several times, and transferred into a 3.2-mm glass tube (Wilmad, Vineland, NJ). The glass tube was sealed with epoxy glue and inserted into a 5-mm MAS rotor.

All of the solid-state NMR spectra were recorded on a 300-MHz CMX300 spectrometer (Chemagnetics; Varian, Palo Alto, CA). The ^{13}C and ^{15}N cross-polarization (CP)-MAS spectra were recorded with a CP contact time of 3 ms and a recycle delay of 2.5 s at 45°C under various MAS frequencies. Two-pulse phase modulation (TPPM) ^{1}H decoupling (20) was applied during acquisition with a decoupling power of 65 kHz.

^{13}C-^{15}N rotational-echo double-resonance NMR (REDOR) spectra were acquired with a 5-mm triple-resonance MAS probe for ^{1}H, ^{13}C, and ^{15}N (Varian) using *xy*-8 phase cycling for ^{15}N irradiations (21). The MAS frequency was 5000 Hz and the rotor temperature was maintained at 45°C. The ^{1}H 90° pulse width was 3.3 μs and the 180° pulse widths for ^{13}C and ^{15}N were 8.5 and 8.3 μs, respectively. The contact time for CP was set to 3 ms. The recycle delay was 2.5 s, the sweep width was 30 kHz, and the number of scans was ~16,000. TPPM ^{1}H decoupling (20) was applied during acquisition with a decoupling power of 65 kHz.

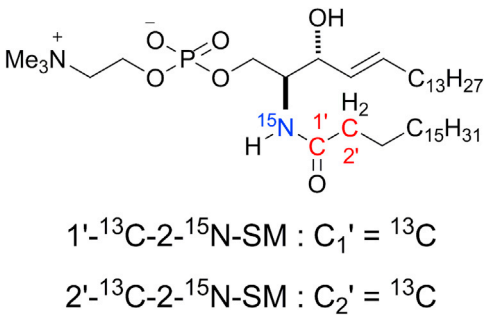

FIGURE 1 Structure of ^{13}C/^{15}N doubly labeled SMs. To see this figure in color, go online.

RESULTS AND DISCUSSION

Preparation of ^{13}C and ^{15}N doubly labeled SMs

An *N*-stearoyl SM was selected for this study because it is the most abundant SM constituent in bovine brain (22). We prepared two types of ^{13}C and ^{15}N doubly labeled SMs (Fig. 1): 1′-^{13}C-2-^{15}N-SM for ^{13}C and ^{15}N CSA and intramolecular dipole coupling measurements, and 2′-^{13}C-2-^{15}N-SM for intramolecular dipole coupling measurements. These labeled SMs were synthesized by coupling ^{13}C-labeled stearic acids with 2-^{15}N-lyso-SM prepared using a modification of a previously reported procedure (Fig. 2) (15,23). Briefly, starting from ^{15}N-L-serine, the formation of a Weireb amide followed by a substitution reaction with a vinyl Grignard reagent provided a vinyl ketone. The ketone was reduced to a secondary alcohol with LiAlH(O*t*-Bu)$_3$ and the resulting allyl alcohol was subjected to olefin metathesis using a Grubbs catalyst.

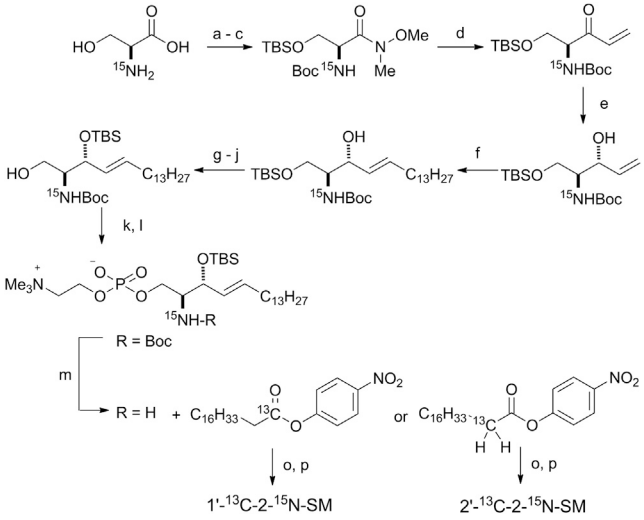

FIGURE 2 Synthesis of ^{13}C/^{15}N doubly labeled SMs. (*a–p*) Reagents and conditions: (*a*) $(Boc)_2O$, NaOH, H_2O, dioxane, rt, 2 h; (*b*) NH(Me)OMe·HCl, NMM, EDC, CH_2Cl_2, −15°C, 4 h; (*c*) TBSCl, imidazole, DMF, rt, 1 h (86% for three steps); (*d*) vinyl MgBr, THF, rt, 1.5 h (86%); (*e*) LiAlH(O^{t}Bu)$_3$, EtOH, −78°C, 2 h (93%); (*f*) 1-pentadecene, Grubbs II catalyst, *p*-quinone, CH_2Cl_2, 55°C, 2 h (64%); (*g*) TBAF, THF, rt, 35 min (93%); (*h*) PivCl, pyridine, −30°C, 2 h (89%); (*i*) TBSOTf, 2,6-lutidine, CH_2Cl_2, 0°C, 30 min; (*j*) DBU, MeOH, rt, 16 h (40% for two steps); (*k*) 2-chloro-1,3,2-dioxaphosphoran-2-oxide, Et_3N, DMAP, benzene, 0°C, 1.5 h; (*l*) Me_3N, CH_3CN, 85°C, 46 h (90% for two steps); (*m*) TFA, CH_2Cl_2, 0°C, 1 h; (*o*) Et_3N, DMAP, THF, rt, 21 h; and (*p*) TBAF, THF, rt, 28 h (53% for three steps).

Introduction of a choline group and deprotection of a Boc group gave TBS-protected 2-^{15}N-lyso-SM. Finally, coupling with the *p*-nitrophenyl ester of 1′-^{13}C-stearic acid or 2′-^{13}C-stearic acid (for details regarding the preparation of these esters, see the Supporting Material) furnished the appropriately labeled SMs (Fig. 2). For the static CSA measurements of powdered samples, we also prepared singly labeled SMs (1′-^{13}C-SM and 2-^{15}N-SM) in the same manner.

^{13}C and ^{15}N CSA of SM amides

With the labeled SMs available, we obtained static solid-state NMR spectra of powdered 1′-^{13}C-SM and 2-^{15}N-SM to determine the original CSA tensor values for the amide ^{13}C and ^{15}N of SM, which have not been documented previously. Spectra were recorded with slow MAS under ^{1}H decoupling, and spinning side band patterns were simulated with SIMPSON 3.0 software (24) (Fig. 3). Table 1 lists the principal CSA values, which are typical of amide bonds (25).

Next, to obtain the CSA principal-axis system with respect to the amide frame, we calculated the CSA tensors using the gauge including atomic orbital (GIAO) method (26). The truncated structure shown in Fig. S1 was used to input data for the calculations. Before performing the CSA tensor calculations, we optimized the structure using Becke's three-parameter hybrid functional (27) and the Lee, Yang, and Parr correlation functional (B3LYP) (28) method using a 6-311G(d) basis set. For CSA tensor calculations using the GIAO method, the density-functional theory (DFT) method was adopted with a 6-311G++(2d,2p) basis. Fig. 4 shows the calculated CSA principal-axis systems (for more details, see Tables S1–S5), in which δ_{33} of ^{13}C and δ_{22} of ^{15}N are perpendicular to the amide plane and the remaining principal axes are on the plane. These tensor directions are consistent with those typical of amide bonds (25).

TABLE 1 Principal CSA values (ppm) for powdered SM amides

	δ_{11}	δ_{22}	δ_{33}	δ_{iso}
^{13}C of SM amide	251 (δ_{11}^{C})	185 (δ_{22}^{C})	93 (δ_{33}^{C})	176
^{15}N of SM amide	210 (δ_{11}^{N})	67 (δ_{22}^{N})	54 (δ_{33}^{N})	110

The possible errors were within ±3 ppm.

Similar measurements were performed in hydrated membrane systems with and without equimolar Chol. Since pure stearoyl SM membrane forms gel phase below the phase transition temperature (44°C) (29), which provides broadened solid-state NMR spectra, it is necessary to measure the spectra above 44°C. In addition, in our previous report (17), we found that there is no critical difference in the ^{2}H NMR spectra of deuterated SM bilayers between 45°C and 50°C in either the presence or absence of Chol; thus, the NMR spectra were recorded at 45°C for SM and SM-Chol membranes. In membrane environments, lipid molecules undergo fast axial rotation, giving rise to an axially symmetric signal pattern that is defined by the two tensor values $\delta\perp$ and $\delta_{//}$. Fig. 5 shows the ^{13}C CP-MAS spectra of 1′-^{13}C-2-^{15}N-SM in hydrated bilayers with SIMPSON simulation spectra, which resulted in estimates for the $\delta\perp$ and $\delta_{//}$ values (Table 2), in conjunction with the anisotropic parameter, $\Delta\delta = \delta_{//} - \delta\perp$. The ^{15}N CSA values of the

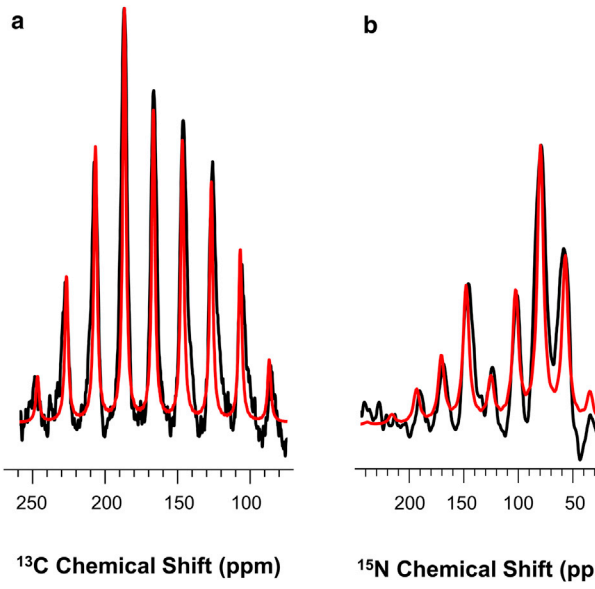

FIGURE 3 (*a* and *b*) Amide regions of CP-MAS spectra (*black lines*) of powdered 1′-^{13}C-SM (*a*) and 2-^{15}N-SM (*b*) with spectral simulation using SIMPSON (*red lines*). Spectra were recorded at 45°C under MAS of (*a*) 1.5 kHz or (*b*) 0.7 kHz. To see this Figure in color, go online.

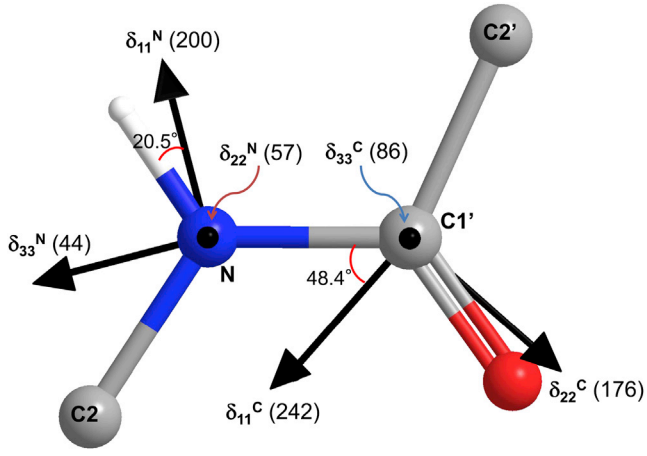

FIGURE 4 Top view of the amide group of SM from calculated ^{13}C and ^{15}N CSA principal-axis systems. The axes of δ_{22}^{N} and δ_{33}^{C} are perpendicular to the amide plane. Experimental principal values in ppm (Table 1) are shown in parentheses. To see this figure in color, go online.

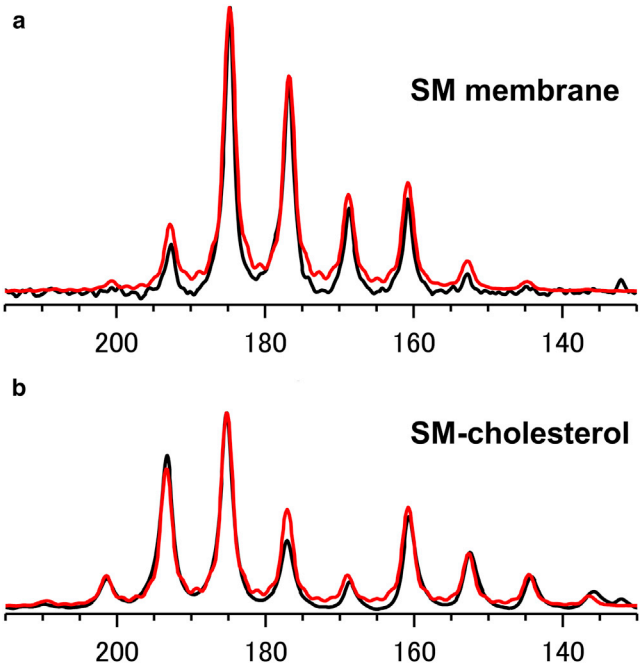

FIGURE 5 ^{13}C CP-MAS spectra of hydrated 1′-^{13}C-2-^{15}N-SM with spectral simulations using SIMPSON (*red lines*). (*a* and *b*) 1′-^{13}C-2-^{15}N-SM (*a*) and 1′-^{13}C-2-^{15}N-SM/Chol (*b*) at a 1:1 molar ratio were hydrated with 50 wt% D_2O, and both spectra were recorded at 45°C under MAS of 600 Hz. To see this figure in color, go online.

SM amide group in membranes were obtained in a similar manner (Table 2; Fig. S2).

Magnitude of the C-N intramolecular dipole coupling of SM amides

Next, to determine the rotational-axis direction and the molecular order parameter of SM amide in bilayers, we measured the intramolecular C-N dipole couplings of 1′-^{13}C-2-^{15}N-SM and 2′-^{13}C-2-^{15}N-SM using the C-N REDOR method (30). Fig. 6 *a* shows the REDOR spectra of the 1′-^{13}C-2-^{15}N-SM/Chol membrane with a dephasing time of 4 ms at 45°C, which demonstrates a significant reduction in the ^{13}C signal due to the intramolecular REDOR dephasing effect from ^{15}N. Fig. 6 *b* plots the experimental REDOR dephasing values ($\Delta S/S_0$) for 1′-^{13}C-2-^{15}N-SM in bilayers. A comparison with theoretical dephasing curves revealed that the intramolecular dipole

TABLE 2 ^{13}C and ^{15}N CSA principal values (ppm) of SM amide in hydrated membranes at 45°C

	^{13}C				^{15}N			
	$\delta_{//}$	$\delta_{\perp}$	$\Delta\delta_C$[a]	δ_{iso}	$\delta_{//}$	$\delta_{\perp}$	$\Delta\delta_N$[a]	δ_{iso}
SM	151.0	188.5	−37.5	176	86	122	−36	110
SM/Chol (1:1)	139.0	194.5	−55.5	176	82	124	−42	110

[a]Anisotropic parameter $\Delta\delta = \delta_{//} - \delta_{\perp}$. The possible errors were within ±3 ppm.

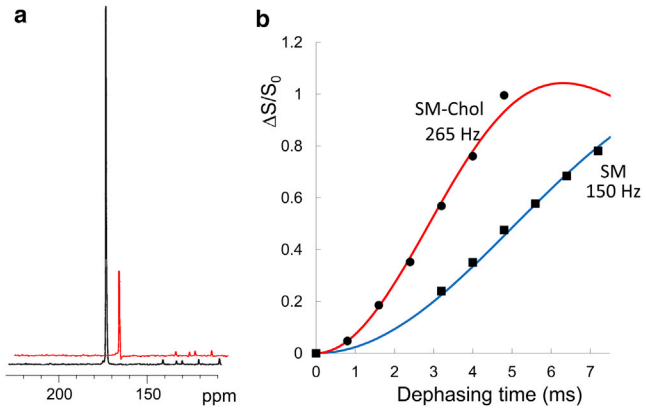

FIGURE 6 Intramolecular REDOR experiments for 1′-^{13}C-2-^{15}N-SM. (*a*) ^{13}C-^{15}N REDOR spectra for the SM-Chol membrane (1′-^{13}C-2-^{15}N-SM/Chol = 1:1 in 50 wt% D_2O) with a dephasing time of 4 ms at 45°C. The S_0 (*black line*) and S (*red line*) spectra were obtained with and without ^{15}N-irradiation, respectively. (*b*) REDOR dephasing effects for (●) SM-Chol membranes and (■) SM-only membranes at various dephasing times. ΔS was ($S_0 - S$). The best-fit theoretical curves were obtained with D = 265 Hz (*red line*) and 150 Hz (*blue line*) for SM-Chol and SM membranes, respectively. The possible errors were within ±20 Hz. To see this figure in color, go online.

coupling values between C1′ and N were 265 and 150 Hz for the SM-Chol and SM membranes, respectively. Note that intermolecular C-N dipole coupling was negligible at these dephasing times because intermolecular REDOR between 1′-^{13}C-SM and 2′-^{15}N-SM was marginal, at most $\Delta S/S_0$ = 2%, even at much longer dephasing times (≥40 ms; unpublished results).

Similarly, the intramolecular REDOR between C2′ and amide N was measured using 2′-^{13}C-2-^{15}N-SM bilayers. As shown in Fig. 7, the intramolecular dipole coupling for SM-Chol was 13 Hz as determined from theoretical curve fitting, whereas the SM membrane did not produce any significant REDOR dephasing effect even at a dephasing time of 160 ms. This suggests that dipole coupling is almost nonexistent, probably because the average angle between the rotation axis and the C2′-N bond is close to the magic angle.

Calculations of the rotation-axis angles and order parameter for SM amides

The rotation axis is defined by the polar coordinates α (azimuthal angle) and β (polar angle) connecting the rotation axis with the ^{13}C CSA tensor axes (Fig. 8). To account for the wobbling of the rotation axis, the order parameter (S), which varies from 1 to 0, was introduced. When S = 1, no molecular wobbling with respect to the rotation axis is present, and when S = 0, every orientation is allowed (such as in solution) (31). Although Saupe order tensor analysis is more exact when the wobbling motion of the rotation axis is anisotropic (32),

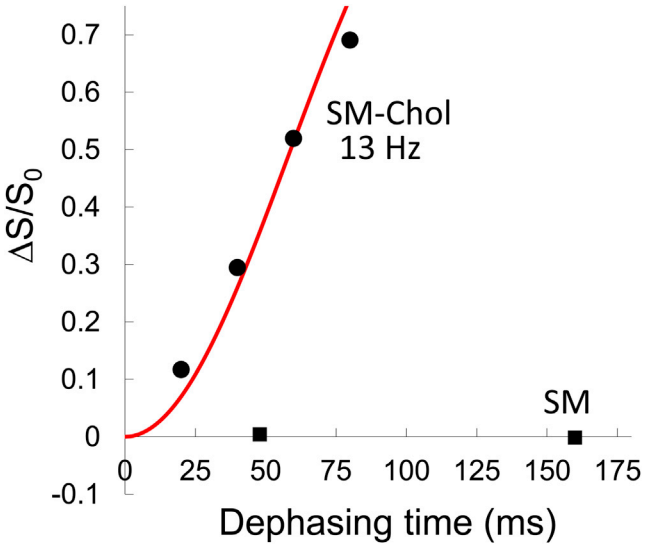

FIGURE 7 Intramolecular REDOR plots for 2′-^{13}C-2-^{15}N-SM in membranes in the (●) presence and (■) absence of Chol. ΔS was ($S_0 - S$). Intramolecular REDOR dephasing was not observed for the SM membrane. The best-fit theoretical curve for SM-Chol with $D = 13$ Hz is shown. The possible errors were within ±2 Hz. To see this figure in color, go online.

approximating the motion using the single order parameter S, which assumes a fast isotropic wobbling, also is acceptable (31).

Using α, β, and S values, the anisotropic parameter of the amide ^{13}C ($\Delta\delta_C^{Calc}$) can be calculated as (18,33)

$$\Delta\delta_C^{Calc} = S \times \left[\delta_{33}^{C}\left(3\cos^2\beta - 1\right) + \delta_{11}^{C}\left(3\sin^2\alpha\sin^2\beta - 1\right) + \delta_{22}^{C}\left(3\sin^2\beta\cos^2\alpha - 1\right)\right]/2.$$

Similarly, as a function of α, β, and S, $\Delta\delta_N^{Calc}$ is given by

$$\Delta\delta_N^{Calc} = S \times \left[\delta_{22}^{N}\left(3\cos^2\beta - 1\right) + \delta_{11}^{N}\left\{3\sin^2(\alpha - 129.4^\circ)\sin^2\beta - 1\right\} + \delta_{33}^{N}\left\{3\sin^2\beta\cos^2(\alpha - 129.4^\circ) - 1\right\}\right]/2,$$

where terms containing ($\alpha - 129.4^\circ$) appear because the δ_{11}^{N} direction overlaps δ_{11}^{C} due to a -129.4° rotation around the normal of the amide plane (Fig. 4).

The magnitude of dipolar coupling is known to depend on molecular motion as well as internuclear distance. Therefore, for a fixed internuclear distance such as C1′-N and C2′-N in the doubly labeled SMs, attenuation of the magnitude of coupling should be due only to motional averaging. When the C1′-N bond vector is rotating around the axis, the C1′-N dipolar coupling constant can be provided by the following equation (31):

$$D_{C1'-N}^{Calc} = D_{C1'-N}^{Static} \times S \times \left(3\cos^2\theta - 1\right)/2,$$

where θ is the angle between the C1′-N vector and the rotation axis (Fig. 8) and $D_{C1'-N}^{Static}$ denotes the dipolar coupling constant for the static C1′-N interaction, which was calculated to be 1303 Hz based on the C1′-N internuclear distance of 1.33 Å. Angle θ is related to α and β by $\cos\theta = \sin\beta\cos(138.4^\circ - \alpha)$ because the angle between the C1′-N vector and δ_{22}^{C} is 138.4° (Fig. 4).

Similarly, the C2′-N dipolar coupling constant is provided by

$$D_{C2'-N}^{Calc} = D_{C2'-N}^{Static} \times S \times \left(3\cos^2\phi - 1\right)/2,$$

where ϕ is the angle between the C2′-N vector and the rotation axis, which has the relation $\cos\phi = \sin\beta\cos(103.8^\circ - \alpha)$, because the angle between the C2′-N vector and δC 22 is 103.8° (Fig. 4). The value for $D_{C2'-N}^{Static}$ was calculated to be 219 Hz based on the C2′-N internuclear distance of 2.41 Å.

The best-fit combinations of α, β, and S were obtained by minimizing the root mean-square deviation (RMSD) between the experimental and calculated dipolar coupling constants D ($D_{C1'-N}$ and $D_{C2'-N}$) and anisotropic parameters $\Delta\delta$ ($\Delta\delta_C$ and $\Delta\delta_N$):

$$RMSD\ (\alpha,\beta,S) = \sqrt{\sum_i\left(\frac{D_i^{Exp} - D_i^{Calc}(\alpha,\beta,S)}{D_{max}}\right)^2 + \sum_i\left(\frac{\Delta\delta_i^{Exp} - \Delta\delta_i^{Calc}(\alpha,\beta,S)}{\Delta\delta_{max}}\right)^2}$$

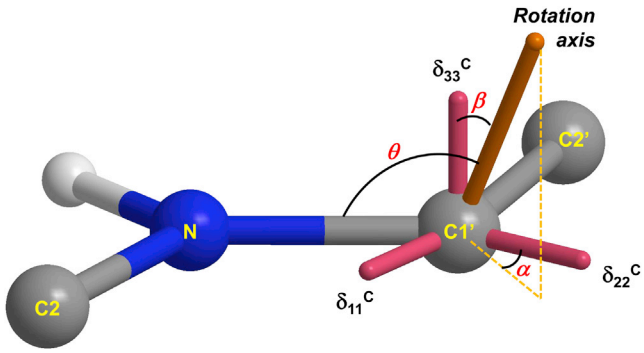

FIGURE 8 The rotation-axis direction is defined by the polar coordinates α (azimuthal angle) and β (polar angle) with respect to the ^{13}C CSA tensor axes. Angle θ is the angle between the rotation axis and the C1′-N bond. The oxygen atom on C1′ was omitted for clarity. To see this figure in color, go online.

Each value in this equation was normalized by its rigid-limit value (D_{max} or $\Delta\delta_{max}$) to equalize the contributions from dipolar couplings and chemical shifts (34).

Fig. 9 shows the 2D RMSD plots for SM and SM-Chol membranes at S values of 0.67 and 0.84, respectively, which provide the minimum RMSD values. From the figure, the combinations of α, β, and S were elucidated as listed in Table 3, although β has two possible values for each membrane. Although Fig. 9 seems to indicate another minimum points at $\alpha = \sim 140°$ and $\beta = \sim 45°$ and 135°, we can rule out these combinations because those RMSD values are 0.10 for SM and 0.16 for SM-Chol membranes, and thus are much higher than those listed in Table 3. It is also clear from the contour gradient in Fig. 9 that α angles in Table 3 have larger uncertainty than β angles. These results indicate that the rotational-axis directions are very similar regardless of the presence or absence of Chol, whereas the order parameter S is enhanced significantly by Chol. The value of S is related to wobbling in the rotation axis, and a value of 0.84 leads to a cone semi-angle of 14° for oscillations of the rotation axis when a Gaussian distribution of the wobbling angle is assumed (35,36). In contrast, an S value of 0.67 indicates an angle of 21°.

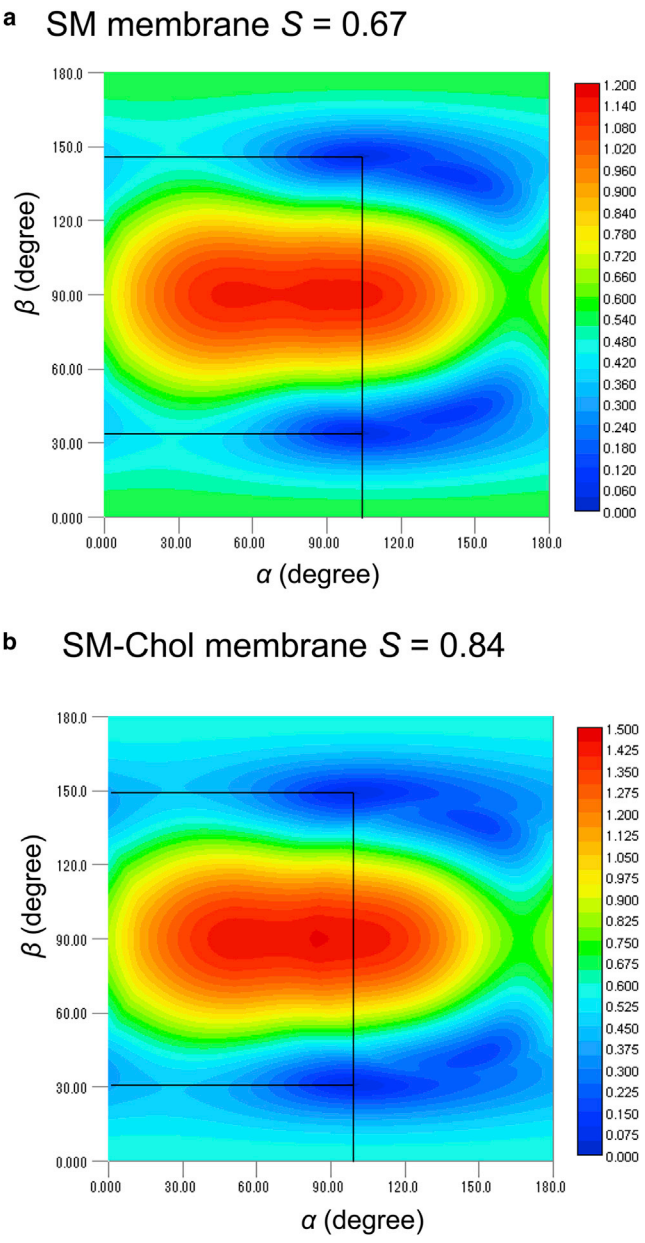

FIGURE 9 (a and b) 2D RMSD contour plots for (a) SM at $S = 0.67$ and (b) SM-Chol at $S = 0.84$; β has two possible values. To see this figure in color, go online.

TABLE 3 Order parameter S and (α, β) values that provide a minimum RMSD

	RMSD	S	α	β[a]
SM	0.03	0.67 ± 0.05	103° ± 10°	34° ± 3° (146 ± 3°)
SM-Chol	0.045	0.84 ± 0.05	99° ± 10°	31° ± 3° (149 ± 3°)

The uncertainties take into account the propagation of experimental errors. [a]Although the two possible β values give two potential rotational-axis directions, the values in the parentheses are less probable when the conformation of SM is considered (see text).

Of note are the small RMSD values in both membranes (Table 3), which validate the current assumption that the wobbling motion of the amide rotation axis is fast and isotropic. As described above, if the wobbling motion of the rotation axis is anisotropic, Saupe order tensor analysis using S_{zz} and $S_{xx}-S_{yy}$ values should be adopted (32), and therefore the approximation using a single order parameter S (i.e., the $S_{xx}-S_{yy}$ value is ignored) would provide much larger RMSD values.

Because of the two possible β values (Fig. 9; Table 3), each membrane has two possible rotational-axis directions. Fig. 10 a shows the two possible orientations of the amide plane of the SM-Chol membrane according to the values listed in Table 3. A recent report revealed that SM forms bicelles with dihexanoylphosphocholine (15), and its partial conformation in bicelles was determined, indicating that the conformation around the amide is relatively stable based on coupling constants typical of anti-rotamers. Based on the conformation of SM, the orientation corresponding to a β of 31° (Fig. 10 b) is more reasonable because the long axis of an SM molecule appears parallel to the rotation axis, whereas the rotation axis is not directed along the SM long axis when β is 149° (Fig. 10 c). Therefore, the rotational axes of SM amide are $\alpha = 103°$, $\beta = 34°$, and $S = 0.67$ for SM bilayers, and $\alpha = 99°$, $\beta = 31°$, and $S = 0.84$ for SM-Chol bilayers.

Implications for amide orientation analysis

Here, we first discuss the validity of the above analysis, in which structural heterogeneity of the amide orientation is assigned entirely to wobble. Judging from the typical static CSA values of SM in the powder state (Table 1), it is reasonable to consider that the amide plane is rigid. On that basis,

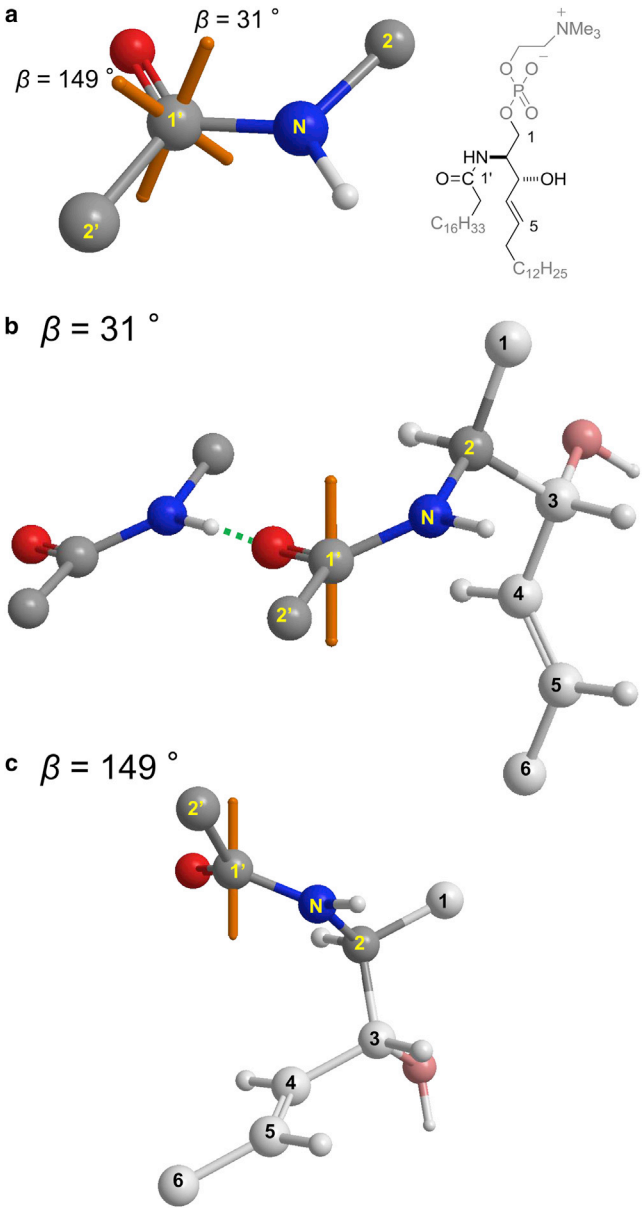

FIGURE 10 (*a–c*) Two rotation-axis directions for an SM-Chol membrane (*a*) with respect to the amide plane and partial orientations of an SM molecule for (*b*) $\beta = 31°$ or (*c*) 149°, based on the conformation of SM deduced from bicelle experiments (15). The orange axes indicate the rotation axes. Considering the direction of an acyl chain, orientation *b* is more likely than *c*. Structure *b* also shows one possible intermolecular hydrogen bond involving the SM amide group. To see this figure in color, go online.

we assumed that the amide plane takes a single major orientation with wobbling. Of course, there are two other possibilities: 1) stable plural orientations of the amide plane exist with respect to the rotation axis and 2) the plural orientations exchange rapidly. The latter case can be regarded as wobbling of the amide plane, and therefore our assumption holds true. The former case would provide larger RMSD values because the calculation of dipolar and anisotropy values in the RMSD equation is based on the assumption that the SM amide takes a single orientation. The small RMSD values (Table 3) suggest that the dynamics of the amide plane can be approximated as a single major orientation with wobbling, although the residual RMSDs might indicate the presence of minor orientations.

SM molecules feature two potential hydrogen-bond donors in the bilayer interfacial region, i.e., amide and hydroxy groups, whereas PCs contain none of these. Consequently, the formation of interlipid hydrogen bonds is often proposed as a mechanism of raft formation (10–14,37–39). Interestingly, this study demonstrates that the SM amide orientation is not affected significantly by the presence or absence of Chol. There are two possible explanations for this: first, the direct hydrogen bonding between the SM amide and Chol may not be as strong as previously proposed. This seems in line with our previous observations (16,17) that Chol is situated more deeply in SM membranes than in saturated PC membranes; more specifically, the rigid alicyclic parts of Chol are located in the middle region of alkyl chains of SM. The resultant depth difference between the SM amide and the Chol OH group would induce an orientational change of the SM amide plane upon formation of the hydrogen bond. A recent simulation study also suggested minimal formation of hydrogen bonds between the SM amide and Chol (40). Second, it is also possible to form a water-bridged hydrogen bond between the SM amide and Chol without significantly altering the amide orientation. On the basis of our data, we are unable to distinguish between these two possibilities; however, detailed simulation studies based on our data may help to resolve this issue.

In contrast, Chol significantly enhanced the order parameter *S* of SM amide from 0.67 to 0.84, indicating that Chol restricts the rotation axis wobbling of the SM amide. A possible explanation for this result is that the interlipid distances were shortened due to the ordering effect of Chol on the SM alkyl chains, consequently promoting the intermolecular hydrogen-bond networks involving the SM amide. In fact, the orientation and conformation around the SM amide, as shown in Fig. 10 *b*, seems suitable for forming intermolecular hydrogen bonds with neighboring SM amides. In other words, Chol is likely to shift the equilibrium toward formation of the amide-associated hydrogen bonds through its ordering effect on the SM alkyl chains. Collectively, the upper regions of SM-Chol membranes appear to be stabilized by the hydrogen bonds involving the SM amide, and the middle regions are ordered by the rigid alicyclic skeleton of Chol, both of which synergistically contribute to form the ordered phase of SM-Chol membranes.

CONCLUSIONS

In this study we revealed the orientation and order parameter of the amide moiety of SM in the presence and

absence of Chol by using C-N dipole couplings and chemical-shift anisotropies, and successfully preparing ^{13}C and ^{15}N doubly labeled SMs. We demonstrated that the amide orientation was minimally affected by Chol, whereas the order was enhanced significantly in the presence of Chol. These findings can be explained by the notion that the ordering effect of Chol on the SM alkyl chains tightens membrane packing, shortens the interlipid distances, and promotes the intermolecular hydrogen bonds involving the SM amide. In fact, the orientation of the SM amide (Fig. 10 *b*), as deduced from the results presented here as well as a previously determined conformation of SM (15), seems suitable for forming the intermolecular hydrogen bonds between SM amides, although it is also possible to form intermolecular hydrogen bonds with the OH group of Chol. The hydrogen bonds thus formed restrict the wobbling of the SM amide and enhance its order. Considering the dynamic nature of bilayer membranes, the SM amide is more likely to rapidly undergo hydrogen-bond formation and dissociation than to form stable intermolecular hydrogen bonds. Therefore, it is more reasonable to assume that the stabilization effect of Chol on the hydrophobic regions of SM shifts the dynamic equilibrium toward intermolecular hydrogen-bond formation involving the SM amide. In this context, this study provides new (to our knowledge) insights into the significance of the SM amide orientation with regard to molecular recognition in lipid rafts, and therefore enhances our understanding of lipid rafts and the mechanism of their formation. Finally, it is expected that the results of this study, in conjunction with previously reported comprehensive deuterium order profiles of SM alkyl chains (16,17,41–43), will provide basic information for molecular-dynamics studies of SM membranes.

SUPPORTING MATERIAL

Supporting Materials and Methods, two figures, and five tables are available at http://www.biophysj.org/biophysj/supplemental/S0006-3495(15)00496-8.

AUTHOR CONTRIBUTIONS

N.M. designed research, T.Y. and Y.M. performed research, and all authors analyzed data. N.M. and M.M. wrote the article.

ACKNOWLEDGMENTS

The authors thank Dr. Naoya Inazumi (Osaka University), Prof. Tohru Oishi (Kyushu University), and Dr. Yuichi Umegawa (Osaka University) for their help with organic synthesis and solid-state NMR measurements.

This work was supported by Grants-in-Aid for Scientific Research (A) (No. 25242073), (B) (No. 20310132), and (S) (No. 18101010) from MEXT, Japan, and by a SUNBOR grant from the Suntory Institute for Bioorganic Research, Japan.

REFERENCES

1. Simons, K., and E. Ikonen. 1997. Functional rafts in cell membranes. *Nature.* 387:569–572.
2. Anderson, R. G. W., and K. Jacobson. 2002. A role for lipid shells in targeting proteins to caveolae, rafts, and other lipid domains. *Science.* 296:1821–1825.
3. Binder, W. H., V. Barragan, and F. M. Menger. 2003. Domains and rafts in lipid membranes. *Angew. Chem. Int. Ed. Engl.* 42:5802–5827.
4. Simons, K., and D. Toomre. 2000. Lipid rafts and signal transduction. *Nat. Rev. Mol. Cell Biol.* 1:31–39.
5. Ikonen, E. 2001. Roles of lipid rafts in membrane transport. *Curr. Opin. Cell Biol.* 13:470–477.
6. Brown, D. A., and E. London. 1998. Functions of lipid rafts in biological membranes. *Annu. Rev. Cell Dev. Biol.* 14:111–136.
7. Ahmed, S. N., D. A. Brown, and E. London. 1997. On the origin of sphingolipid/cholesterol-rich detergent-insoluble cell membranes: physiological concentrations of cholesterol and sphingolipid induce formation of a detergent-insoluble, liquid-ordered lipid phase in model membranes. *Biochemistry.* 36:10944–10953.
8. Baumgart, T., S. T. Hess, and W. W. Webb. 2003. Imaging coexisting fluid domains in biomembrane models coupling curvature and line tension. *Nature.* 425:821–824.
9. Silvius, J. R., D. del Giudice, and M. Lafleur. 1996. Cholesterol at different bilayer concentrations can promote or antagonize lateral segregation of phospholipids of differing acyl chain length. *Biochemistry.* 35:15198–15208.
10. Simons, K., and W. L. C. Vaz. 2004. Model systems, lipid rafts, and cell membranes. *Annu. Rev. Biophys. Biomol. Struct.* 33:269–295.
11. Li, X.-M., M. M. Momsen, …, R. E. Brown. 2001. Cholesterol decreases the interfacial elasticity and detergent solubility of sphingomyelins. *Biochemistry.* 40:5954–5963.
12. Bittman, R., C. R. Kasireddy, …, J. P. Slotte. 1994. Interaction of cholesterol with sphingomyelin in monolayers and vesicles. *Biochemistry.* 33:11776–11781.
13. Sankaram, M. B., and T. E. Thompson. 1990. Interaction of cholesterol with various glycerophospholipids and sphingomyelin. *Biochemistry.* 29:10670–10675.
14. Zidar, J., F. Merzel, …, D. Janežic. 2009. Liquid-ordered phase formation in cholesterol/sphingomyelin bilayers: all-atom molecular dynamics simulations. *J. Phys. Chem. B.* 113:15795–15802.
15. Yamaguchi, T., T. Suzuki, …, M. Murata. 2012. NMR-based conformational analysis of sphingomyelin in bicelles. *Bioorg. Med. Chem.* 20:270–278.
16. Matsumori, N., T. Yasuda, …, M. Murata. 2012. Comprehensive molecular motion capture for sphingomyelin by site-specific deuterium labeling. *Biochemistry.* 51:8363–8370.
17. Yasuda, T., M. Kinoshita, …, N. Matsumori. 2014. Detailed comparison of deuterium quadrupole profiles between sphingomyelin and phosphatidylcholine bilayers. *Biophys. J.* 106:631–638.
18. Matsumori, N., Y. Kasai, …, K. Nomura. 2008. Orientation of fluorinated cholesterol in lipid bilayers analyzed by ^{19}F tensor calculation and solid-state NMR. *J. Am. Chem. Soc.* 130:4757–4766.
19. Matsumori, N., H. Okazaki, …, M. Murata. 2011. Fluorinated cholesterol retains domain-forming activity in sphingomyelin bilayers. *Chem. Phys. Lipids.* 164:401–408.
20. Bennett, A. E., C. M. Rienstra, …, R. G. Griffin. 1995. Heteronuclear decoupling in rotating solids. *J. Chem. Phys.* 103:6951–6958.
21. Gullion, T., D. B. Baker, and M. S. Conradi. 1990. New, compensated Carr-Purcell sequences. *J. Magn. Reson.* 89:479–484.
22. Jungalwala, F. B., V. Hayssen, …, R. H. McCluer. 1979. Separation of molecular species of sphingomyelin by reversed-phase high-performance liquid chromatography. *J. Lipid Res.* 20:579–587.

23. Yamamoto, T., H. Hasegawa, …, S. Katsumura. 2006. Versatile synthetic method for sphingolipids and functionalized sphingosine derivatives via olefin cross metathesis. *Org. Lett.* 8:5569–5572.

24. Bak, M., J. T. Rasmussen, and N. C. Nielsen. 2000. SIMPSON: a general simulation program for solid-state NMR spectroscopy. *J. Magn. Reson.* 147:296–330.

25. Saitô, H., I. Ando, and A. Ramamoorthy. 2010. Chemical shift tensor—the heart of NMR: insights into biological aspects of proteins. *Prog. Nucl. Magn. Reson. Spectrosc.* 57:181–228.

26. Ditchfield, R. 1974. Self-consistent perturbation theory of diamagnetism 1. A gauge-invariant LCAO method for NMR chemical shifts. *Mol. Phys.* 27:789–807.

27. Becke, A. D. 1993. Density-functional thermochemistry. III. The role of exact exchange. *J. Chem. Phys.* 98:5648–5652.

28. Lee, C., W. Yang, and R. G. Parr. 1988. Development of the Colle-Salvetti correlation-energy formula into a functional of the electron density. *Phys. Rev. B Condens. Matter.* 37:785–789.

29. Jaikishan, S., A. Björkbom, and J. P. Slotte. 2010. Sphingomyelin analogs with branched *N*-acyl chains: the position of branching dramatically affects acyl chain order and sterol interactions in bilayer membranes. *Biochim. Biophys. Acta.* 1798:1987–1994.

30. Gullion, T., and J. Schaefer. 1989. Rotational-echo double-resonance NMR. *J. Magn. Reson.* 81:196–200.

31. Ulrich, A. S. 2005. Solid state F-19 NMR methods for studying biomembranes. *Prog. Nucl. Magn. Reson. Spectrosc.* 46:1–21.

32. Sternberg, U., R. Witter, and A. S. Ulrich. 2007. All-atom molecular dynamics simulations using orientational constraints from anisotropic NMR samples. *J. Biomol. NMR.* 38:23–39.

33. Bechinger, B., and C. Sizun. 2003. Alignment and structural analysis of membrane polypeptides by ^{15}N and ^{31}P solid-state NMR spectroscopy. *Concepts Magn. Reson. A.* 18A:130–145.

34. Tang, M., A. J. Waring, …, M. Hong. 2006. Orientation of a β-hairpin antimicrobial peptide in lipid bilayers from two-dimensional dipolar chemical-shift correlation NMR. *Biophys. J.* 90:3616–3624.

35. Shaikh, S. R., V. Cherezov, …, S. R. Wassall. 2006. Molecular organization of cholesterol in unsaturated phosphatidylethanolamines: X-ray diffraction and solid state ^{2}H NMR reveal differences with phosphatidylcholines. *J. Am. Chem. Soc.* 128:5375–5383.

36. Oldfield, E., M. Meadows, …, R. Jacobs. 1978. Spectroscopic studies of specifically deuterium labeled membrane systems. Nuclear magnetic resonance investigation of the effects of cholesterol in model systems. *Biochemistry.* 17:2727–2740.

37. Khelashvili, G. A., and H. L. Scott. 2004. Combined Monte Carlo and molecular dynamics simulation of hydrated 18:0 sphingomyelin-cholesterol lipid bilayers. *J. Chem. Phys.* 120:9841–9847.

38. Veiga, M. P., J. L. R. Arrondo, …, D. Marsh. 2001. Interaction of cholesterol with sphingomyelin in mixed membranes containing phosphatidylcholine, studied by spin-label ESR and IR spectroscopies. A possible stabilization of gel-phase sphingolipid domains by cholesterol. *Biochemistry.* 40:2614–2622.

39. Epand, R. M. 2003. Cholesterol in bilayers of sphingomyelin or dihydrosphingomyelin at concentrations found in ocular lens membranes. *Biophys. J.* 84:3102–3110.

40. Zhang, Z., S. Y. Bhide, and M. L. Berkowitz. 2007. Molecular dynamics simulations of bilayers containing mixtures of sphingomyelin with cholesterol and phosphatidylcholine with cholesterol. *J. Phys. Chem. B.* 111:12888–12897.

41. Bunge, A., P. Müller, …, D. Huster. 2008. Characterization of the ternary mixture of sphingomyelin, POPC, and cholesterol: support for an inhomogeneous lipid distribution at high temperatures. *Biophys. J.* 94:2680–2690.

42. Bartels, T., R. S. Lankalapalli, …, M. F. Brown. 2008. Raftlike mixtures of sphingomyelin and cholesterol investigated by solid-state ^{2}H NMR spectroscopy. *J. Am. Chem. Soc.* 130:14521–14532.

43. Veatch, S. L., O. Soubias, …, K. Gawrisch. 2007. Critical fluctuations in domain-forming lipid mixtures. *Proc. Natl. Acad. Sci. USA.* 104:17650–17655.